JOURNAL OF SOLID STATE CHEMISTRY 111, 208–216 (1994)

Electronic Structure of Perovskite Oxides, $LaMO_3$ (M = Ti–Ni), from High-Energy Electron Spectroscopic Investigations

D. D. Sarma and A. Chainani

Solid State and Structural Chemistry Unit, Indian Institute of Science, Bangalore 560012, India

Received November 15, 1993; in revised form March 3, 1994; accepted March 4, 1994

IN HONOR OF C. N. R. RAO ON HIS 60TH BIRTHDAY

We study the electronic structure of the $LaMO_3$ (M = Ti–Ni) perovskite oxides as probed by various high-energy electron spectroscopies. These spectroscopic studies, in conjunction with model many-body calculations, provide important information concerning the ground state character of these oxides. In particular, the on-site Coulomb interaction strength, U_{dd}, the charge transfer energy, Δ, and the transfer integral between the metal $3d$ and oxygen $2p$ states, t, have been estimated. These parameters are found to exhibit a systematic variation across the series. Electronic structure of the perovskites is discussed in terms of electron-removal and electron-addition spectra for the parent compound as well as for doped $LaMO_3$, with specific reference to semiconductor–metal transitions.

INTRODUCTION

The metallic or insulating properties of transition metal compounds in general, and oxides in particular, have often been described in terms of the Zaanen–Sawatzky–Allen(ZSA) phase diagram (1). The essential aspect of this phase diagram is to rationalize the properties in terms of three interaction paramcters, namely the charge transfer energy, Δ, between the metal $3d$ and ligand p states, the intra-atomic Coulomb interaction strength, U_{dd}, within the transition metal $3d$ manifold, and the transfer integral, t, between the metal $3d$ and ligand p states. It was shown that for small values of U_{dd}/t, one obtains an essentially d-band metal, while for small values of Δ/t, a mixed valent p–d metal is obtained. For larger values of U_{dd} and Δ, a Mott–Hubbard insulator or a charge transfer insulator is obtained, depending on whether $\Delta > U_{dd}$ or $U_{dd} > \Delta$. This phase diagram was calculated within an impurity model. Subsequent calculations (2, 3) based on a multiband Hubbard model also yielded a similar phase diagram but with the evidence of a new insulating phase, the covalent insulator, which was not realized in the ZSA diagram. There are some obvious advantages (2, 3) in describing transition metal compounds in terms of a multiband model instead of an impurity model, as only a multiband model can take into account the bandwidths of the Hubbard bands and also provide a meaningful description of the magnetic structure.

The $3d$ transition metal oxides are known to have a wide range of electronic and magnetic properties and, more interestingly, many of these oxides exhibit spectacular electronic and magnetic transitions as a function of temperature, pressure, and/or composition (4). Such a wide spectrum of properties is a direct consequence of a competition for dominance between the three interactions U_{dd}, Δ, and t. A study of the perovskite oxide series, $LaMO_3$, with M = Ti–Ni is best suited to the purpose of investigating this competition. The entire series forms in closely related structures. While $LaTiO_3$ is a small band gap semiconductor which readily becomes metallic in presence of oxygen nonstoichiometry (5, 6), $LaMO_3$ with M = V–Co are insulators (7–11). The last member in the series, $LaNiO_3$, is a strongly correlated metal (12). The magnetic properties are also varied; for example, $LaTiO_3$ is weakly ferromagnetic (5), while $LaMO_3$ with M = V–Fe are antiferromagnetic (7–11). While no magnetic ordering has been observed in $LaCoO_3$, it exhibits a spin-state transition as a function of temperature (13). $LaNiO_3$ exhibits strongly enhanced Pauli paramagnetic susceptibility (12). Most of the insulating stoichiometric compounds in this series undergo an insulator–metal transition in the presence of hole doping in terms of Sr^{2+} substitution for La^{3+} or in the presence of excess oxygen; e.g., $La_{1-x}Sr_xTiO_3$ (6), $LaTiO_{3+\delta}$ (5), $La_{1-x}Sr_xVO_3$ (7), $La_{1-x}Sr_xMnO_3$ (9), $LaMnO_{3+\delta}$ (14), and $La_{1-x}Sr_xCoO_3$ (11). Among these, the case of $La_{1-x}Sr_xMnO_3$ is highly anomalous (15). Many of these series also exhibit an antiferromagnetic to ferromagnetic transition, while $La_{1-x}Sr_xCoO_3$ has a nonmagnetic to ferromagnetic transition. It is also possible to induce a metal–insulator transition in these systems by homovalent substitutions, i.e., without any electron or hole doping, in

0022-4596/94 $6.00

contrast to the case of heterovalent substitutions discussed above. Examples of such systems are homovalent substituted $LaNi_{1-x}M_xO_3$ with M = Mn, Fe, or Co (16).

The above discussion shows that these perovskite oxides are an interesting class of related compounds with a wide variety of properties. Moreover, U_{dd} is expected to increase and Δ is expected to decrease across the transition metal series. This leads to the situation that $LaMO_3$ compounds span the entire range of electronic properties categorized in terms of ZSA or the modified ZSA phase diagrams. Thus, $LaTiO_3$ is a nearly metallic d-band system, $LaVO_3$ and $LaCrO_3$ are Mott–Hubbard insulators, while $LaMnO_3$–$LaCoO_3$ have a strongly mixed character, with $LaCoO_3$ being closer to the charge transfer insulator region. Finally, $LaNiO_3$ is a mixed-valent p–d metal. The example of a covalent insulator is found in the closely related compound, $NdNiO_3$ (17).

Photoemission spectroscopy and other high-energy spectroscopic investigations have contributed significantly to our understanding of the physical properties of these compounds. Analysis of the spectroscopic data in terms of model calculations, including configuration interaction, has provided estimates of U_{dd}, Δ, and t, allowing a systematic description of the electronic structure of these compounds. We shall discuss these aspects critically, based on high-energy spectroscopic studies of these compounds.

RESULTS AND DISCUSSION

We show X-ray photoelectron (XP) spectra (17–22) of the valence band regions in $LaMO_3$ (M = Ti, Cr–Ni) in Fig. 1. Ultraviolet photoelectron (UP) spectra using He I and He II radiations have also been reported in the literature (17, 19–22). One such UP spectrum is shown for $LaCoO_3$ in the inset of Fig. 1. A comparison of this UP spectrum with the corresponding XP spectrum shows some obvious changes in the spectral shape and intensity. Specifically, the intensity of spectral features close to E_F decreases relative to the intensity of the high binding energy peak in every case (17, 20–22), as can be observed for the case of $LaCoO_3$ in Fig. 1. It is known (23) that the photoionization probability of transition metal $3d$ states, compared to the oxygen $2p$ states, increases with increasing photon energy; this suggests that the spectral features close to E_F arise primarily from photoemission of metal $3d$ states in all these compounds, with the high binding energy feature near 6 eV arising from states with primarily oxygen $2p$ character. While the spectral shape near the O $2p$ region is expected to be dominated by band structure effects, the spectral features related to the metal $3d$ derived states have been explained in terms of the ionic multiplet structure of the photoionized $3d^{n-1}$ final state configuration (18). While

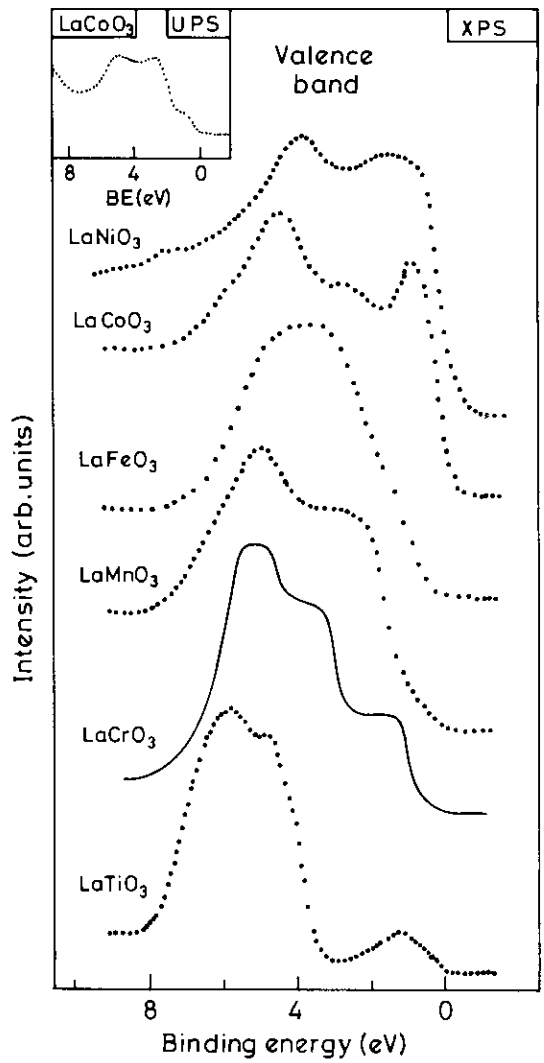

FIG. 1. The XPS valence band spectra of $LaMO_3$ (M = Cr–Ni). The $LaCrO_3$ spectrum is adapted from Ref. (18). The $LaTiO_3$ spectrum, obtained with a photon energy of 48 eV is adapted from Ref. (19). The zero of the binding energy scale corresponds to the Fermi level. Inset shows the He I spectrum of $LaCoO_3$.

such an approach appears to account for the spectra at least qualitatively, it does not take into account covalency effects or effects arising from configuration interaction. In general, the transfer integrals coupling the metal $3d$ to the oxygen $2p$ states are comparable to the charge-transfer energies as well as to the intra-atomic Coulomb interaction strengths in the case of $LaMO_3$ compounds. This implies that both the covalency effect and the configuration interaction will have substantial contributions in determining the ground state electronic structure. Besides the $3d$ related feature, primarily oxygen $2p$ derived peaks at higher binding energies show interesting variation across the series (Fig. 1). In particular, the energy position of this peak systematically shifts to lower binding energy as shown in Fig. 1. Thus, the O $2p$ peak ap-

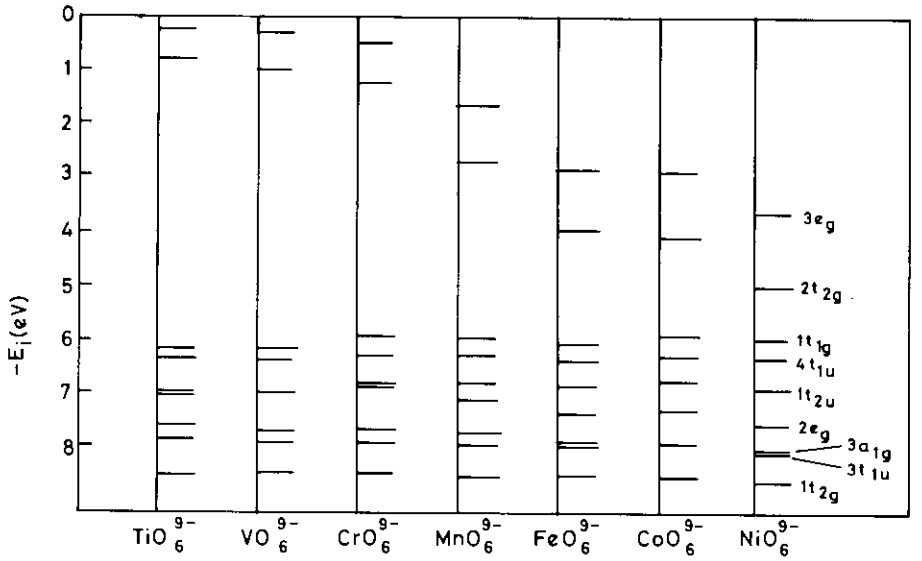

FIG. 2. The energy level diagram obtained for MO_6^{9-} octahedra from MSXα calculations.

pears at about 7.1 eV binding energy in $LaTiO_3$, while it is at 4.5 eV in $LaNiO_3$. This effect is related to the increasing stabilization of the metal $3d$ state relative to the oxygen $2p$ state, leading to a decrease of the charge transfer energy, $\Delta = E(d^{n+1}p^{m-1}) - E(d^n p^m)$, across the series.

The above discussed trend in the energetics can also be observed in the electronic structure calculations for the MO_6^{9-} octahedra (24). The energy level diagram for the molecular orbitals obtained from multiscattering Xα (MSXα) calculations for these octahedra (24) are shown in Fig. 2. In every case, the primarily oxygen $2p$ derived states are found to be between 6 and 8.5 eV with a centroid at about 7.2 eV. On the other hand, the binding energies of the metal $3d$ derived t_{2g} and e_g states (denoted as $2t_{2g}$ and $3e_g$ in Fig. 2) systematically increase with increasing atomic number of the transition metal. Thus, the $2t_{2g}$ level in TiO_6^{9-} octahedra appears at about 1 eV, while it is at about 5 eV in the case of NiO_6^{9-} cluster (Fig. 2). In the case of these compounds all the oxygen $2p$ derived states are fully filled. The Fermi energy of the system is then determined by the number of d-electrons of the M^{3+} ion in $LaMO_3$, and these electrons are distributed in the metal-derived t_{2g} and e_g levels. While the results shown in Fig. 2 are based on spin-restricted calculations, exchange splitting will lift the degeneracy of the up- and down-spin states in the presence of a finite-spin configuration. Thus, in the cases of $LaTiO_3$, $LaVO_3$, and $LaCrO_3$, the t_{2g} level is partly occupied and the e_g level is entirely empty. In the case of $LaMnO_3$ and $LaFeO_3$, a larger exchange stabilization energy compared to the crystal-field splitting leads to the high-spin configuration with both t_{2g} and e_g partly occupied. For the last two compounds in this series, $LaCoO_3$ and $LaNiO_3$, a low-spin ground state leads to a fully filled t_{2g} level with the remaining d-electron in the case of $LaNiO_3$ having an e_g character. Accordingly the Fermi energy in each of these compounds will be in the t_{2g} or e_g derived bands. Thus, the shift in energy of the t_{2g} and e_g levels toward the oxygen $2p$ derived states in Fig. 2 will appear as a shift of the oxygen $2p$ derived band toward the Fermi energy across the series, as illustrated in the photoemission valence band spectra in Fig. 1.

It is, however, to be noted that the above discussion is based on a single-particle description of the electronic structure. Such a description expectedly fails to explain the ground state properties of these compounds. For example, the above description would imply that all the $LaMO_3$ compounds should be metallic, whereas all these except for $LaNiO_3$ are, in fact, insulating. It is, however, to be noted that $LaCoO_3$, with the low-spin t_{2g}^6 configuration may become a band insulator, if the crystal-field splitting is larger than the d-bandwidths. Similarly, there is a possibility of deriving an insulating ground state in $LaFeO_3$, if the up-spin t_{2g} and e_g bands are fully separated from the down-spin bands due to a large exchange splitting. Furthermore, $LaCrO_3$ could become an insulator with its $t_{2g\uparrow}^3$ configuration, provided both the crystal-field strength, and the exchange splitting are large compared to the d-bandwidths. However, even such a one-particle description is likely to have difficulty in explaining the existence of large bandgaps in these systems. Thus it appears that the insulating ground states in these compounds are dependent on the existence of a large intra-atomic Coulomb interaction strength within the $3d$ manifold. High-energy spectroscopy has been very useful in estimating this quantity, and we shall discuss this in a

later section. Here we point out that it is, however, possible to drive these insulating stoichiometric $LaMO_3$ to a metallic state by doping of charge carriers, as discussed earlier. Many such systems have been investigated in detail using various high-energy spectroscopic techniques (17, 20–22). We show X-ray photoelectron spectra in the valence band regions of $La_{1-x}Sr_xMO_3$ with M = Mn, Fe, and Co for $x = 0.4$ in Fig. 3. The spectra from the $La_{1-x}Sr_xCoO_3$ (with $x = 0.0$ in Fig. 1. and $x = 0.4$ in Fig. 3) show several differences. For example, there is a distinct shift of the oxygen $2p$ related peak position from 5.2 eV with $x = 0.0$ to 4.9 eV with $x = 0.4$ (compare Figs. 1 and 3). This shift can be easily understood by noting that the substitution of La by Sr leads to doping the system with holes. These holes would populate the top of the occupied band, moving E_F to lower energy. Thus, in the valence band spectrum, we should indeed expect to see a shift of the O $2p$ related feature towards E_F. In contrast, such a shift of the oxygen $2p$ binding energy is not observed for $La_{0.6}Sr_{0.4}FeO_3$ or $La_{0.6}Sr_{0.4}MnO_3$, (Fig. 3) compared to the undoped samples (Fig. 1). This suggests that the doped hole states split off from top of the occupied band and are localized above it by the potential of the dopant. If the localization of the doped states were to be due only to disorder effects (Anderson localization) without involving any splitting off of the doped hole states, the Fermi energy would still be lowered, reflected in a corresponding shift of the oxygen $2p$ binding energy. However, such a shift is not seen in the experimental spectra for these two series (Fig. 3).

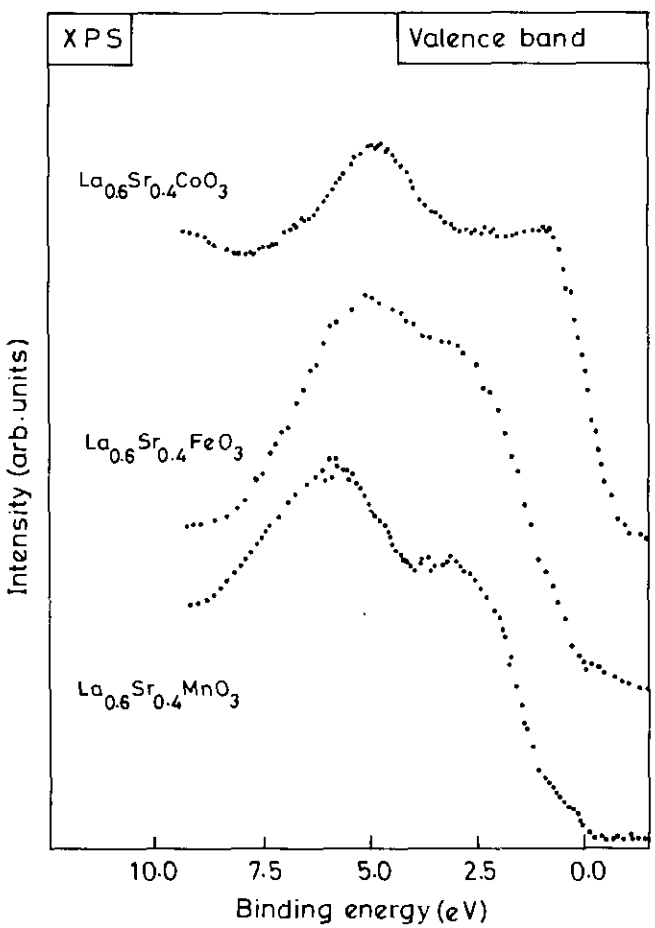

FIG. 3. The XPS valence band spectra of $La_{0.6}Sr_{0.4}MO_3$ for M = Mn, Fe, and Co.

The splitting off of the doped hole states from top of the occupied states would imply that there will not be any spectral intensity at E_F in the valence band photoemission spectra. We show the valence band photoemission spectra with better resolution, using He I radiation for the compounds $La_{1-x}Sr_xCoO_3$ and $La_{1-x}Sr_xMnO_3$ with $x = 0.0$ and 0.4 and for $La_{0.6}Sr_{0.4}FeO_3$, in Fig. 4. We could not record reproducible UP spectra for $LaFeO_3$ due to severe charging effects. The stoichiometric compounds with $x = 0.0$ exhibit no intensity at E_F in all the three cases, consistent with their semiconducting/insulating behaviour. On Sr substitution, $La_{1-x}Sr_xCoO_3$ clearly exhibits a finite spectral intensity at E_F, indicating a transition to the metallic state. In contrast, the spectrum of $La_{0.6}Sr_{0.4}FeO_3$ exhibits no spectral intensity at E_F, in accordance with the discussion above and consistent with the semiconducting behavior of this compound. The most puzzling situation, however, is encountered in the case of $La_{1-x}Sr_xMnO_3$. The He I valence band spectrum of $La_{0.6}Sr_{0.4}MnO_3$ (Fig. 4) is very similar to that of $LaMnO_3$, with no perceivable intensity at E_F. This observation is consistent with the fact that the oxygen $2p$ related binding energy does not shift on Sr substitution (Fig. 3), indicating a splitting off of the dope hole states from the top of the occupied band. But these observations are not in agreement with the metallic properties of this composition [15]. One possibility is that the finite density of states (DOS) at E_F, which is responsible for the metallic properties of $La_{1-x}Sr_xMnO_3$ with $x \geq 0.2$, is too low to be detected within the sensitivity of photoemission spectroscopy. Such an interpretation would be consistent with the observation of a relatively large value of resistivity even for the conducting samples [15].

We note here that the above mentioned M–I transitions are brought about by hole doping. Thus, while photoemission spectra probing the occupied part of the density of states exhibit some changes, the dope hole states are expected to be seen directly on probing the unoccupied part of the DOS. We show the Bremsstrahlung isochromat (BI) spectra of some of the compounds in Fig. 5. From this figure it is clear that new hole states are generated at E_F in Sr-doped $LaCoO_3$ (22), consistent with the metallic conductivity of these samples and the UP spectra shown in Fig. 4. On the other hand, substitution of Sr for La in $LaMnO_3$ does not lead to any perceivable spec-

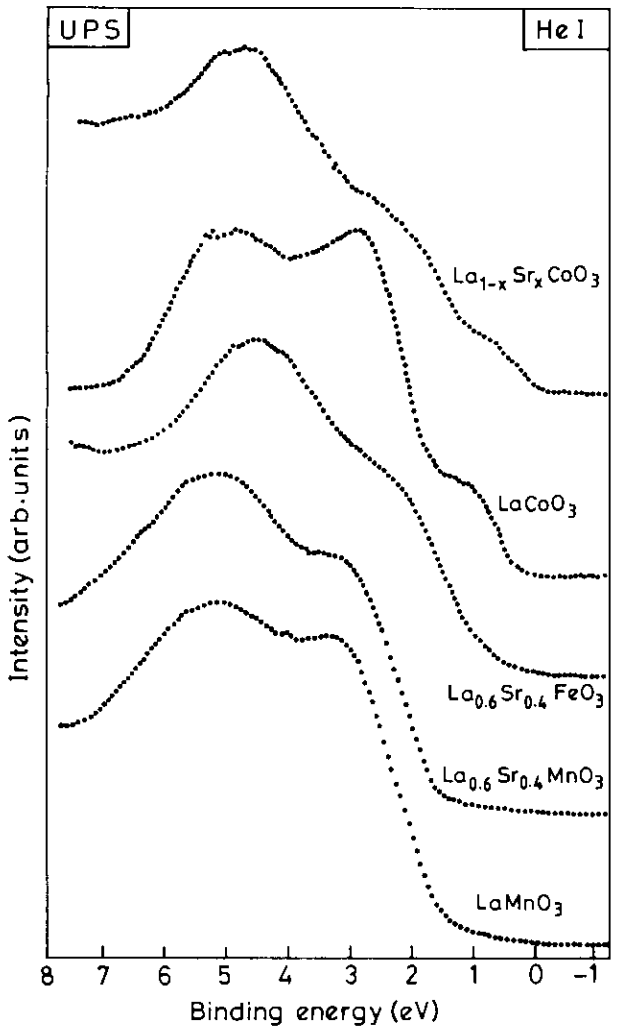

FIG. 4. , The He I spectra for $La_{1-x}Sr_xMO_3$ (M = Mn, Co; x = 0.0 and 0.4) and $La_{0.6}Sr_{0.4}FeO_3$.

tral intensity at E_F (Fig. 5). A close inspection of the spectral features in $La_{1-x}Sr_xMnO_3$ (20) suggests that the doped hole states exist with a peak at about 1.2 eV above E_F with negligible intensity at E_F. This is consistent with the photoemission spectra of this series (Fig. 4), suggesting a very low carrier density for the metallic compositions. BI spectra of $La_{1-x}Sr_xFeO_3$ (21) shown in Fig. 5 also suggest that the doped hole states are localized above E_F, in agreement with the insulating property of $La_{1-x}Sr_xFeO_3$.

As discussed above, the occupied and unoccupied parts of DOS probed by photoemission and Bremsstrahlung isochromat spectroscopies provide a qualitative description of the electronic structure and the M–I transitions in these series. In order to provide a quantitative description, it is necessary to obtain estimates of various electronic strengths, such as the charge transfer energy (Δ), the transfer integrals between the metal 3d and oxygen 2p (t) and the intra-atomic Coulomb interaction within the transition metal 3d manifold (U_{dd}). It is possible to estimate U_{dd} directly from the transition metal L_3–$M_{45}M_{45}$ Auger spectra. The final state of such an Auger process has two holes in the metal 3d manifold. These two holes can be localized at the same site and thus interact with each other with U_{dd}. However, there is another possible final state with the two holes at two different atomic sites and thus screened from each other. The spectral signature of the second possibility with two uncorrelated holes corresponds to the self-convolution of the occupied part of the DOS and is separated from the spectal signature of the correlated final state by U_{dd}. In general, one obtains the spectral signatures for both these

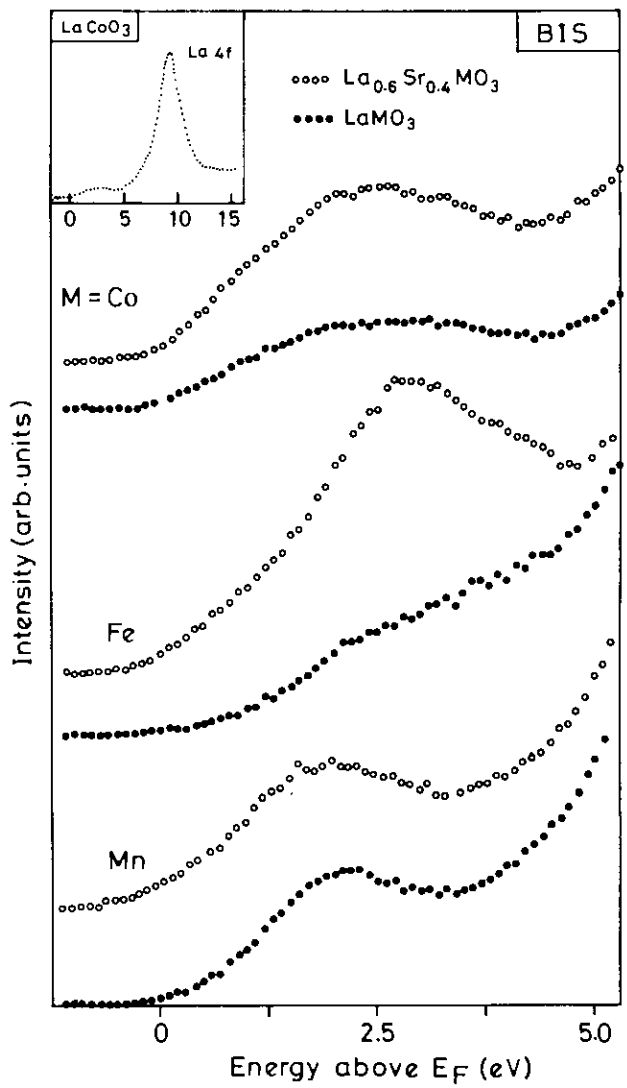

FIG. 5. The BI spectra for $La_{1-x}Sr_xMO_3$ (M = Mn, Fe and Co; x = 0.0 and 0.4). The inset shows the wide range BI spectrum for $LaCoO_3$ showing La 4f states.

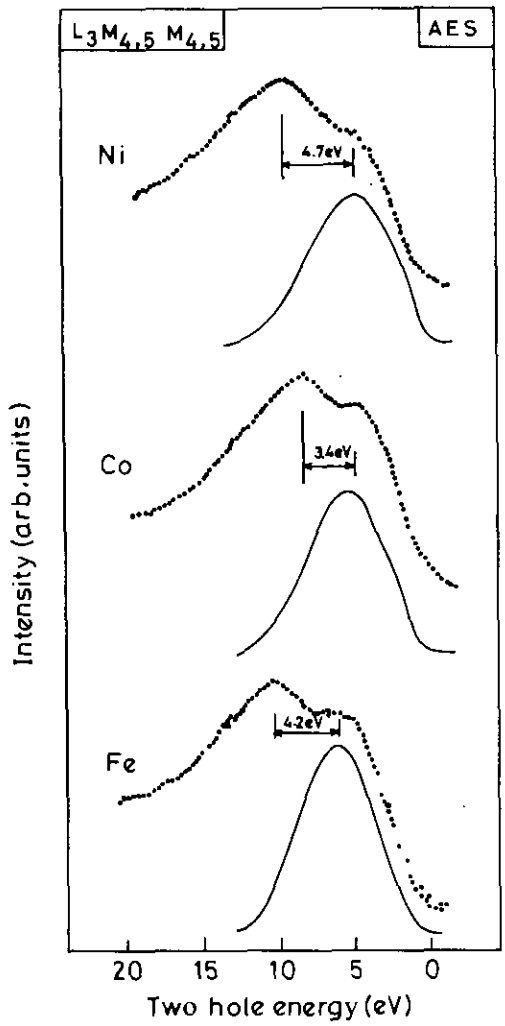

FIG. 6. The metal L_3–$M_{45}M_{45}$ Auger spectra for M = Fe, Co and Ni, compared with the self-convoluted XPS valence band spectra plotted on the two hole energy scale.

final states. We show the L_3–$M_{45}M_{45}$ Auger spectra of $LaNiO_3$, $LaCoO_3$, and $La_{0.6}Sr_{0.4}FeO_3$, compared with the respective self-convoluted DOS, in Fig. 6. In each case, it is found that the self-convoluted DOS describes the higher kinetic energy spectral features very well, suggesting its origin from two uncorrelated holes in the final state. Thus the peak at lower kinetic energy, which has no counterpart in the self-convolution, is attributed to the spectral signature of a correlated two hole final state. U_{dd} is then directly estimated from the energy difference of these two experimental features as shown in Fig. 6. The estimate of U_{dd} in the Ni and Co $3d$ states is found to be 4.7 and 3.4 eV, respectively, while for Fe $3d$ states it is estimated to be about 4.2 eV. It should be noted that the U_{dd} estimated from the Auger spectra for the case of $LaFeO_3$, besides including the hybridization shifts, relates to the transition $d^5 \rightarrow d^3$ and is given by $(U-J)$, where U and J are the direct and exchange Coulomb interaction strengths. On the other hand, the Hubbard U^H_{dd} corresponds to a transition $2d^5 \rightarrow d^6 + d^4$ and this is given by $(U + 4J)$. Thus the U^H_{dd} relevant for the ground state charge fluctuations in a d^5 case is $5J$ larger than that estimated from Auger spectra. Using an estimate of J (= 0.8 eV) from BI spectra (21) we obtain U^H_{dd} ($2d^5 \rightarrow d^6 + d^4$) to be about 8.2 ± 0.5 eV. It should be noted that the large difference between the U_{dd} estimated from Auger spectra and the U^H_{dd} corresponding to the transition $2d^n \rightarrow d^{n+1} + d^{n-1}$ exists only for n corresponding to the half-filled case.

The other two electronic strengths, Δ and t, are readily estimated from an analysis of the metal $2p$ core level photoemission spectra. We show the experimental metal M $2p$ core level spectra (17, 18, 20–22) of $LaMO_3$ (M = Ti, Cr–Ni) in Fig. 7. The core level spectrum of $LaVO_3$

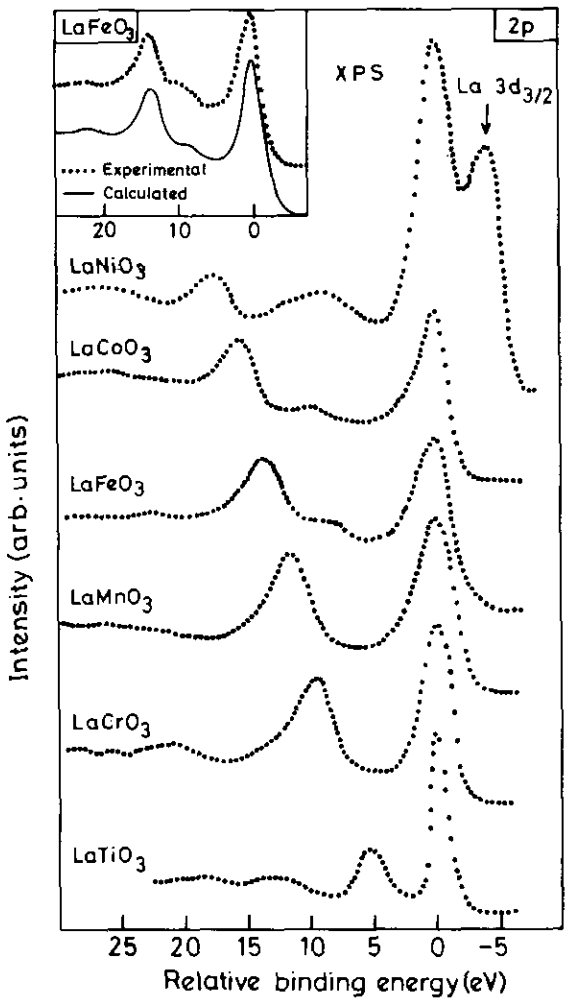

FIG. 7. The metal M $2p$ core level spectra for $LaMO_3$ (M = Ti, Cr–Ni). Inset shows the comparison with the calculated spectrum for $LaFeO_3$. The spectra for $LaTiO_3$ and $LaCrO_3$ are adapted from Ref. (18).

has not been reported in the literature. It is to be noted that the Ni $2p$ spectrum in $LaNiO_3$ is extensively overlapped by La $3d_{3/2}$ spectral features, particularly on the lower binding energy side. In every case shown in Fig. 7 one can notice two well-defined spectral features in the spectra corresponding to spin–orbit split $2p_{3/2}$ and $2p_{1/2}$ states. The intensities of these two spectral features are in the ratio of 2 : 1, being governed by the $(2J + 1)$ degeneracy of the final states. Besides these two prominent features, weaker satellite features can also be observed in the spectra. These satellite features accompany both the $2p_{3/2}$ and the $2p_{1/2}$ spectral features on the higher binding energy side. While the main peaks in the spectra correspond to the lowest energy final state with a core hole, the satellite features represent transitions into excited states. The origin of the satellite feature may be either intrinsic or extrinsic to the photoionization process. In the case of the intrinsic satellite generation, the intensities are given by the sudden approximation and the process is modelled including the core-hole potential (25). An extrinsic satellite originates due to inelastic processes and consequent energy loss of the photoexicted electron during its transport to the sample surface. Since the intrinsic satellite includes the effect of core-hole generation, the satellite features are expected to be very different depending on whether it accompanies the metal core level or the ligand core level. On the other hand, the extrinsic loss processes are relatively insensitive of the nature of the photoexited core level. The satellite structure observed in $LaTiO_3$ is very similar to that in $SrTiO_3$, with comparable intensity and energy separation (26). These appear to be extrinsic in nature. This is supported by the observation of an energy loss feature in the electron energy loss spectrum of $SrTiO_3$ at nearly the same energy separation as the energy separation between the main peak and the satellite in the core-level spectrum (26). Moreover, satellite features with similar energy separation between the main and the satellite peaks are found to accompany all the core levels, and in particular the oxygen 1s core level. It appears to us that the satellite structure observed in $LaCrO_3$ may also be due to an extrinsic loss process, though it is not very clear at the moment. Electron energy loss spectrum of $LaCrO_3$ will help to identify the origin of the satellite. On the other hand, the core level spectra of $LaMO_3$ with M = Mn–Ni exhibit intrinsic satellite structures (Fig. 7) which have been analyzed within a cluster model including configuration interaction (17, 20–22). The core level spectrum is calculated using a model Hamiltonian including the interaction parameters U_{dd}^H, Δ, and t, in order to simulate the experimental results. The best fit provides estimates for various electronic parameter strengths. A more detailed description of such calculations can be found in Ref. (22). We show one such comparison between the calculated and the experimental spectra for the case of $LeFeO_3$ in the inset of Fig. 7; as can be seen in this inset, the calculation provides a very good description for the experimental spectra. The thus obtained estimates of the charge transfer energy, Δ, the transfer integral, t, and the Coulomb interaction strength, U_{dd}^H (estimated from Auger spectra, as discussed earlier), are shown in Table 1. Since configuration interaction is included in these calculations, the ground state of the system is described as a linear combination of different configurations, such as d^n, $d^{n+1}\underline{L}^1$ and $d^{n+2}\underline{L}^2$, where $\underline{L}$ represents a ligand (oxygen $2p$) hole state. In Table 1 we also indicate the relative contributions of these configurations in the ground state.

Table 1 shows several interesting variations across the series. The charge-transfer energy, Δ, exhibits an overall decreasing trend across the series, in agreement with the MSXα results shown in Fig. 2. We point out here that the calculated spectra are relatively insensitive to changes in Δ, and thus the estimates of Δ are somewhat uncertain. On the other hand, the transfer integral, t, is very well estimated from these analyses, since the calculated spectrum depends quite sensitively on it. The suggested values of t are uncertain to less than ± 0.2 eV. We find that t decreases smoothly across the $3d$ series, being 3.8 eV for $LaMnO_3$ and 3.3 eV for $LaNiO_3$. The strength of the intra-atomic Coulomb interaction within the transition metal $3d$ manifold, U_{dd}^H, is expected to increase across the series. However, this expectation is not fully justified by the U_{dd}^H values in Table 1. For example, U_{dd}^H in the case of $LaFeO_3$ is much larger than that in the other $LaMO_3$ compounds. This large increase of U_{dd}^H for $LaFeO_3$ arises due to the $3d^5$ configuration having an extra contribution of $5J$, as pointed out earlier. With the estimate of J shown in Table 1, U_{dd}, without this extra contribution, would have been 4.2 eV (see Fig. 6); this value follows the slow increasing trend of U_{dd} across the series. However, U_{dd} for $LaCoO_3$ is 3.4 eV, smallest in the $LaMO_3$

TABLE 1

	$LaMnO_3$ d^4	$LaFeO_3$ d^5	$LaCoO_3$ d^6	$LaNiO_3$ d^7
d^n	50.0%	47.5%	43.0%	37.6%
$d^{n+1}\underline{L}^1$	41.0%	43.3%	45.0%	50.1%
$d^{n+2}\underline{L}^2$	9.05	8.7%	12.05%	11.8%
Δ	5.0 eV	4.0 eV	4.0 eV	1.5 eV
t_σ	3.8 eV	3.5 eV	3.4 eV	3.3 eV
U_{dd}^H	4.0 eV	8.2 eV	3.4 eV	4.7 eV
J	0.5 eV	0.8 eV	0.5 eV	1.0 eV
U_{pp}	6.8 eV	6.8 eV	6.7 eV	7.0 eV

Note. The typical estimated errors for the interaction parameters Δ, t_σ, U_{dd}^H, J, and U_{pp} are ± 1.0, ± 0.2, ± 0.5, ± 0.5, and ± 0.5 eV, respectively.

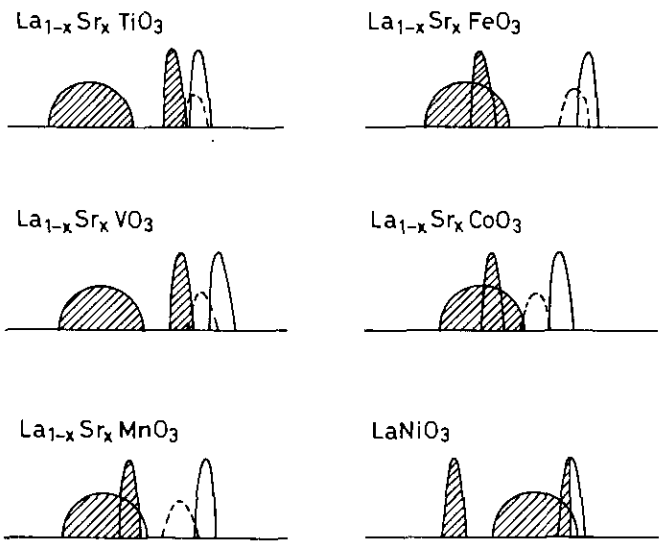

FIG. 8. The schematic electron-removal (hatched) and -addition spectra for $LaMO_3$ (M = Ti, V, Mn–Ni). The dashed curve represents the doped hole states.

series with M = Mn–Ni. We believe that this reduction of U_{dd} in $LaCoO_3$ is due to stronger covalency effects in the low-spin configuration of the ground state giving rise to a more effective screening of charge fluctuations. The Coulomb interaction strength within the oxygen $2p$ states, U_{pp}, estimated from K–$L_{2,3}L_{2,3}$ Auger spectra, is found to be 6.8 ± 0.5 eV for the entire series. The ground state characters in terms of d^n, $d^{n+1}\underline{L}^1$, and $d^{n+2}\underline{L}^2$ configurations vary systematically across the series, arising from the smooth variations of the various electronic parameters (Table 1). It is seen that the majority configuration in the ground state of $LaMnO_3$ is d^4, though there is a nearly equal contribution from $d^5\underline{L}^1$ and $d^6\underline{L}^2$ configurations together. This suggests that covalency effects are strong even for $LaMnO_3$. Though the charge transfer energy, Δ, is slightly larger than the Coulomb correlation strength U_{dd}, $LaMnO_3$ will have to be classified as an insulator belonging to the mixed character region between the Mott–Hubbard insulator and the charge-transfer insulator regions (2). From $LaMnO_3$ till $LaNiO_3$, the d^n contribution to the ground state decreases monotonically, while the contributions of $d^{n+1}\underline{L}^1$ and $d^{n+2}\underline{L}^2$ configurations increase. The end-member of the series, $LaNiO_3$, is a mixed valent p–d metal (17). The estimates of various interaction strengths in $LaMO_3$ compounds having thus been established, the electronic structure in this series can be discussed schematically in terms of electron-removal and electron-addition spectra. We point out here that the various interaction strengths for $LaMO_3$ with M = Ti, V, and Cr have not yet been estimated from the spectroscopic results, though one expects U_{dd} to decrease and charge transfer energy, Δ, to increase for decreasing atomic number of the transition metal, in conformity with the trend shown in Table 1 for M = Mn–Ni. With this in mind, we show the schematic electron-addition and removal spectra for the entire series in Fig. 8. The hatched part represents the electron-removal spectra (the occupied density of states), while the remaining part is the electron-addition spectra (unoccupied density of states). The partially filled $3d$ derived states of the transition metal split into a fully occupied narrow lower Hubbard band and an empty upper Hubbard band separated by approximately U_{dd}. The semicircular occupied density of states represents the relatively broad oxygen $2p$ derived band. In $LaMO_3$ compounds of the early transition elements, the charge transfer energy, Δ, is larger than U_{dd}, leading to the situation shown for $LaTiO_3$. The stoichiometric compound is a small gap insulator (5, 6), the gap being essentially controlled by the strength of U_{dd} and the bandwidths of the Hubbard bands. Thus, these compounds belong to the Mott–Hubbard insulator region. In the case of $LaCrO_3$, we expect U_{dd} to be larger than that in the neighboring $LaVO_3$ and $LaMnO_3$. This is expected since the $t_{2g}^3\uparrow$ configuration of Cr^{3+} represents a half-filled case due to substantial exchange and crystal-field splittings. The situation here is quite similar to that in $LaFeO_3$, which also exhibits an anomalously large U_{dd}. The energy to add an electron to the $t_{2g}\downarrow$ state in the presence of $t_{2g}^3\uparrow$ of Cr^{3+} has an extra contribution from the exchange splitting, and to add it to the $e_g\uparrow$ state requires the extra energy due to the crystal-field splitting. This in effect pushes up the upper Hubbard band, leading to a larger band gap than in the neighboring oxides. Across the series, Δ decreases while U_{dd} increases; this brings in the oxygen $2p$ related bandwidth in between the two Hubbard bands for the late transition metal compounds. In this limit the bandgap is controlled more by the charge transfer energy Δ than by U_{dd}. However, for these compounds ($LaMO_3$ with M = Mn, Fe and Co), both U_{dd}/t and Δ/t are of the order of unity, leading to a very mixed character of the insulating ground state. In this regime, the strength of the transfer integrals also has considerable influence on the bandgap. The end-member of the series considered here, $LaNiO_3$, has a Δ smaller than the oxygen bandwidth, and thus the empty Hubbard band overlaps the top of the occupied oxygen $2p$ band, leading to a mixed valent metal (17). We can also schematically represent the effect of doping holes by the substitution of Sr in place of La in $La_{1-x}Sr_xMO_3$ or by presence of excess oxygen in $LaMO_{3+\delta}$. These doped hole states are marked with a dashed line in Fig. 8. In the case of $La_{1-x}Sr_xTiO_3$, the doped hole states readily overlap the occupied lower Hubbard band, giving rise to a metal–insulator transition. A very similar situation is also encountered in the case of $La_{1-x}Sr_xVO_3$. In both these

cases the Fermi energy lies in states with primarily metal d character. In the case of $LaCrO_3$ and $LaFeO_3$, the bandgap is large and the doped hole states appear to form considerably above the highest occupied states. There is sufficient spectroscopic evidence (21) that this is indeed the case for $La_{1-x}Sr_xFeO_3$, and we expect the situation to be similar in $La_{1-x}Sr_xCrO_3$. This effect is responsible for the absence of an insulator–metal transition in these two systems. The situation with $La_{1-x}Sr_xMnO_3$ is quite anomalous, as pointed out in the discussion of the valence band spectra. The spectroscopic results suggest that the doped hole states are primarily above E_F; no perceptible DOS could be observed in the experiment, though for $x \geq 0.2$, the system is metallic. Thus it appears that there is a very low DOS at E_F in the case of $La_{1-x}Sr_xMnO_3$, in conformity with the spectroscopic results and the high resistivity of these compounds, even in the metallic phase. In the case of $La_{1-x}Sr_xCoO_3$, the doped hole states overlap the top of the oxygen $2p$ band, leading to an insulator to metal transition for $x \geq 0.2$.

In conclusion, we have presented detailed electron spectroscopic results for $LaMO_3$ and $La_{1-x}Sr_xMO_3$ with M = Ti–Ni. The spectra from the valence band region help to understand the nature of the insulator–metal transition and the electronic structure of these oxides. Auger spectra provide estimates of U_{dd}, while analysis of the transition metal core-level spectra in terms of configuration interaction provides estimates of Δ and t. With the help of these results, the ground state character of the stoichiometric compounds could be evaluated. The electronic structure of the parent and the doped compounds are summarized schematically in terms of electron-removal and addition spectra.

ACKNOWLEDGMENTS

It gives us great pleasure to dedicate this article to Professor C. N. R. Rao, whose continued support and encouragement made most of the work reported here possible. We thank S. R. Barman, M. Mathew, S. Nimkar, and N. Shanthi for collaborative work.

REFERENCES

1. J. Zaanen, G. A. Sawatzky, and J. W. Allen, *Phys. Rev. Lett.* **55,** 418 (1985).
2. D. D. Sarma, H. R. Krishnamurthy, S. Nimkar, S. Ramasesha, P. P. Mitra, and T. V. Ramakrishnan, *Pramana J. Phys.* **38,** L531 (1992); D. D. Sarma, *J. Solid State Chem.* **88,** 45 (1990).
3. S. Nimkar, D. D. Sarma, H. R. Krishnamurthy, and S. Ramasesha, *Phys. Rev. B* **48,** 7355 (1993).
4. J. B. Goodenough, *in* "Progress in Solid State Chemistry" C. H. Reiss, Ed.), Vol. 5, p. 45. Pergamon, London, 1971; C. N. R. Rao and J. Gopalakrishnan, "New Directions in Solid State Chemistry." Cambridge University Press, Cambridge, 1986.
5. F. Lichtenberg, D. Widmer, J. G. Bednorz, T. Williams, and A. Reller, *Z. Phys. B* **82,** 211 (1991); D. A. Crandles, T. Timusk, and J. E. Greedan, *Phys. Rev. B* **44,** 13,250 (1991).
6. Y. Tokura, Y. Taguchi, Y. Okada, Y. Fujishima, T. Arima, K. Kumagai, and Y. Iye, *Phys. Rev. Lett.* **70,** 2126 (1993).
7. P. Dougier and P. Hagenmuller, *J. Solid State Chem.* **15,** 158 (1975).
8. J. B. Webb, M. Sayer, and A. Mansingh, *Can. J. Phys.* **55,** 1725 (1977); K. P. Bansal, S. Kumari, B. K. Das, and G. C. Jain, *J. Mater. Sci.* **18,** 2095 (1983); D. P. Karim and A. T. Aldred, *Phys. Rev. B* **20,** 2255 (1979).
9. J. H. Van Santen and G. H. Jonker, *Physica* **16,** 599 (1950); G. H. Jonker and J. H. Van Santen, *Physica* **19,** 120 (1953).
10. J. Grenier, N. Ea, M. Pouchard, and M. M. Abou-Sekkina, *Mater. Res. Bull.* **19,** 1301 (1984).
11. G. H. Jonker and J. H. Van Santen, *Physica* **16,** 337 (1950); V. G. Bhide, D. S. Rajoria, C. N. R. Rao, G. Rama Rao, and V. G. Jadhao, *Phys. Rev. B* **12,** 2832 (1975).
12. K. Sreedhar, J. M. Honig, M. Darwin, M. McElfresh, P. M. Shand, J. Xu, B. C. Crooker, and J. Spalek, *Phys. Rev. B* **46,** 6382 (1992); K. P. Rajeev, G. V. Shivashankar, and A. K. Raychaudhuri, *Solid State Commun.* **79,** 591 (1991).
13. W. C. Koehler and E. O. Wollan, *J. Phys. Chem. Solids* **2,** 100 (1957); G. Thornton, B. C. Tofield, and A. W. Hewat, *J. Solid State. Chem.* **61,** 301 (1988).
14. M. Verelst, N. Rangavittal, and C. N. R. Rao, *J. Solid State Chem.* **104,** 74 (1993).
15. A. Chainani, M. Mathew, D. D. Sarma, I. Das, and E. V. Sampathkumaran, *Physica B* **186–188,** 995 (1993).
16. C. N. R. Rao, O. Prakash, and P. Ganguly, *J. Solid State Chem.* **15,** 186 (1975); P. Ganguly, N. Y. Vasanthacharya, and C. N. R. Rao, *J. Solid State Chem.* **54,** 400 (1984).
17. S. R. Barman, A. Chainani, and D. D. Sarma, *Phys. Rev. B* **49,** 8475 (1994).
18. B. W. Veal and D. J. Lam, *J. Appl. Phys.* **49,** 1461 (1978); D. J. Lam, B. W. Veal, and D. E. Ellis, *Phys. Rev. B* **22,** 5730 (1980).
19. A. Fujimori, I. Hase, M. Nakamura, H. Namatame, Y. Fujishima, Y. Tokura, M. Abbate, F. M. de Groot, M. T. Czyzyk, J. C. Fuggle, O. Strebel, F. Lopez, M. Domke, and G. Kaindl, *Phys. Rev. B* **46,** 9841 (1992).
20. A. Chainani, M. Mathew, and D. D. Sarma, *Phys. Rev. B* **47,** 15,397 (1993).
21. A. Chainani, M. Mathew, and D. D. Sarma, *Phys. Rev. B* **48,** 14,818 (1993).
22. A. Chainani, M. Mathew, and D. D. Sarma, *Phys. Rev. B* **46,** 9976 (1992).
23. J. J. Yeh and I. Lindau, *At. Data Nucl. Data Tables* **32,** 1 (1985).
24. D. D. Sarma, A. K. Santra, and C. N. R. Rao, *J. Solid State Chem.* **110,** 402 (1994).
25. D. D. Sarma and A. Taraphder, *Phys. Rev. B* **39,** 1570 (1989); D. D. Sarma and S. G. Ovchinnikov, *Phys. Rev. B* **42,** 6817 (1990); J. Park, S. Ryu, M. Han, and S. J. Oh, *Phys. Rev. B* **37,** 10867 (1988); A. E. Bocquet, T. Mizokawa, T. Saitoh, H. Namatame, and A. Fujimori, *Phys. Rev. B* **46,** 3771 (1992).
26. S. R. Barman and D. D. Sarma, unpublished.